DOI 10.1002/pmic.201200562 *Proteomics* 2013, *13*, 1672–1686

RESEARCH ARTICLE

Proteome profiling of exosomes derived from human primary and metastatic colorectal cancer cells reveal differential expression of key metastatic factors and signal transduction components

Hong Ji[1], David W. Greening[1], Thomas W. Barnes[2], Justin W. Lim[2], Bow J. Tauro[1,2], Alin Rai[1], Rong Xu[1], Christopher Adda[1], Suresh Mathivanan[1], Wei Zhao[3], Yanhong Xue[3], Tao Xu[3], Hong-Jian Zhu[4] and Richard J. Simpson[1]*

[1] Department of Biochemistry, La Trobe Institute for Molecular Science, La Trobe University, Melbourne, Victoria, Australia
[2] Department of Biochemistry and Molecular Biology, The University of Melbourne, Melbourne, Victoria, Australia
[3] Institute of Biophysics, Chinese Academy of Sciences, Beijing, P. R. China
[4] Department of Surgery, The University of Melbourne, Melbourne, Victoria, Australia

Received: December 14, 2012
Revised: March 8, 2013
Accepted: March 26, 2013

Exosomes are small extracellular 40–100 nm diameter membrane vesicles of late endosomal origin that can mediate intercellular transfer of RNAs and proteins to assist premetastatic niche formation. Using primary (SW480) and metastatic (SW620) human isogenic colorectal cancer cell lines we compared exosome protein profiles to yield valuable insights into metastatic factors and signaling molecules fundamental to tumor progression. Exosomes purified using OptiPrep™ density gradient fractionation were 40–100 nm in diameter, were of a buoyant density ~1.09 g/mL, and displayed stereotypic exosomal markers TSG101, Alix, and CD63. A major finding was the selective enrichment of metastatic factors (MET, S100A8, S100A9, TNC), signal transduction molecules (EFNB2, JAG1, SRC, TNIK), and lipid raft and lipid raft-associated components (CAV1, FLOT1, FLOT2, PROM1) in exosomes derived from metastatic SW620 cells. Additionally, using cryo-electron microscopy, ultrastructural components in exosomes were identified. A key finding of this study was the detection and colocalization of protein complexes EPCAM-CLDN7 and TNIK-RAP2A in colorectal cancer cell exosomes. The selective enrichment of metastatic factors and signaling pathway components in metastatic colon cancer cell-derived exosomes contributes to our understanding of the cross-talk between tumor and stromal cells in the tumor microenvironment.

Keywords:
Cell biology / Exosomes / Metastasis / Protein complex / Secretome / Cancer

Additional supporting information may be found in the online version of this article at the publisher's web-site

Correspondence: Professor Richard J. Simpson, Department of Biochemistry, La Trobe Institute for Molecular Science (LIMS) Room 113, Physical Sciences Building 4, La Trobe University, Bundoora, Victoria 3086, Australia
E-mail: Richard.Simpson@latrobe.edu.au
Fax: +61-03-9479-1226

Abbreviations: CM, culture media; **CRC**, colorectal cancer; **ECM**, extracellular matrix; **EM**, electron microscopy; **GRB2**, growth factor receptor-bound protein 2; **ITS**, insulin-transferrin-selenium; **sMVs**, shed microvesicles; **SS**, soluble secreted; **TNC**, Tenascin C

*Current address: Justin W. Lim, ABSciex, 10 Biopolis Road, #03-06 Chromos Singapore 138670

Colour Online: See the article online to view Figs. 2 and 5 in colour.

1 Introduction

Accumulating evidence highlights the critical role of the tumor microenvironment during the initiation and progression of carcinogenesis [1, 2]. Insights gained from the crosstalk between the tumor and its surrounding support tissue (the tumor stroma), are being utilized to understand cancer biology and improve molecular diagnostics and therapeutics [1, 3, 4]. Carcinomas are a complex milieu of tumor epithelial cells situated in a microenvironment comprising multiple nonmalignant, albeit genetically altered, cell types such as fibroblasts, endothelial cells, and leukocytes. These diverse cell types communicate, either physically by direct interaction or via the secretion of paracrine signaling molecules (i.e. the secretome). For example, cancer cells and other cells in the tumor microenvironment can modulate angiogenesis, a critical step in cancer progression, either through increased release of proangiogenic factors or reduced secretion of antiangiogenic factors, or by indirectly modulating the extracellular matrix [5, 6]. In addition to secreting soluble proteins into the tumor microenvironment, it is now well established that diverse cell types in the tumor stroma also release a variety of extracellular membrane vesicles, including exosomes, shed microvesicles (sMVs), and apoptotic bodies [7, 8]. Of particular interest, is the accumulating evidence suggesting that systemic factors (soluble–secreted proteins and exosomes) drive, directly or indirectly, formation of the premetastatic niche—a specialized microenvironment created at the sites of future metastases (e.g. sentinel lymph nodes)—that permits survival and outgrowth of disseminated cancer cells [6, 9–12].

Exosomes are small (40–100 nm) membrane vesicles of endocytic origin secreted by a variety of cell types in vitro [7, 13, 14] and found in various body fluids such as blood, bile, urine, malignant ascites, bronchoalveolar lavage fluid, synovial fluid, and breast milk [7, 13, 14]. In addition to proteins shared by exosomes from diverse cell types, they also contain specific subsets of proteins that reflect parental cell functions [7, 13]. Exosomes also contain oncogenic proteins [15], signaling molecules [16, 17] (for a recent review [18]), lipids [19], mRNAs, and microRNAs [20–22] that can be horizontally transferred to recipient cells and regulate their function [21]. Like cellular membrane proteins, subclasses of exosomal membrane proteins are also organized into functional lipid raft microdomains [23–25].

To gain insights into the molecular events of colorectal cancer (CRC) metastasis, we compared the proteome profiles of the soluble secretome and exosomes released from two isogenic human colorectal cancer cell lines (primary SW480 cell line and its lymph node metastatic variant SW620) [26]. Proteome analysis of the exosomes from this in vitro metastatic model has revealed differential expression of key metastatic factors (e.g. MET, S100A8, S100A9, TNC) and signal transduction components such as EFNB2, EGFR, JAG1, SRC, TNIK.

2 Materials and methods

2.1 Materials

SW480 cells were from Ludwig Institute for Cancer Research Ltd. (Parkville Branch, Melbourne) and SW620 cells were from Dr. Liz Vincan (Peter MacCallum Cancer Centre, Australia) [26]. All media and supplements were from Life Technologies (NY, USA). OptiPrep™ was from Axis-Shield PoC (Norway). Mouse anti-TSG101, mouse anti-TNIK, mouse anti-HSP70, mouse anti-Flotillin 1, and mouse anti-E-Cadherin antibodies were from BD Transduction Laboratories (NJ, USA), mouse anti-Alix was from Cell Signaling Technology (MA, USA), rabbit anti-Src antibody was from Life Technologies (NY, USA), and mouse anti-β-Catenin was from Upstate Biotechnology (NY, USA). Goat Claudin 7 antibody and mouse anti-EpCAM were from Santa Cruz Biotechnology (CA, USA).

2.2 Cell culture

SW480 and SW620 cells were routinely cultured in RPMI-1640 medium supplemented with 10% FCS, 60 μg/mL benzylpenicillin and 100 μg/mL streptomycin at 37°C and 10% CO_2 atmosphere. For exosome isolation, approximately 2×10^6 cells were seeded into 150 mm diameter culture dishes (30 dishes per cell line) containing 25 mL of the routine culture medium and cultured until cell density reached 70% confluency. Cells were washed four times with RPMI-1640 medium and then cultured in 15 mL RPMI-1640 medium supplemented with 0.8% insulin-transferrin-selenium (ITS), 60 μg/mL benzylpenicillin and 100 μg/mL streptomycin for 24 h before the collection of cell culture medium (CM). 2F2B mouse endothelial cells were cultured in DMEM supplemented with 10% v/v FCS and 1% v/v P/S.

2.3 Secretome and exosome purification

Secretome and exosome samples were prepared as outlined in Fig. 1A. CM was collected and centrifuged at 480 × *g* for 5 min and 2000 × *g* for 10 min to remove floating cells and cell debris, respectively. The supernatant was further centrifuged at 10 000 × *g* for 30 min at 4°C to pellet sMVs as previously described [27]. Crude exosomes were prepared by ultracentrifugation of the supernatant at 100 000 × *g* for 1 h at 4°C. Soluble-secreted fractions (SS) were obtained as described [28] by filtration through a 0.1 μm syringe filter membrane (Pall, Cornwall, UK) and concentrated to ~1 mL using a 5 K cut-off Amicon Ultra-15 centrifugal filter device (Millipore, Billerica, MA). Seppro™ transferrin IgY microbeads (Genway Biotech, San Diego, CA) were used to deplete the abundant transferrin additive (from ITS) in the SS fraction.

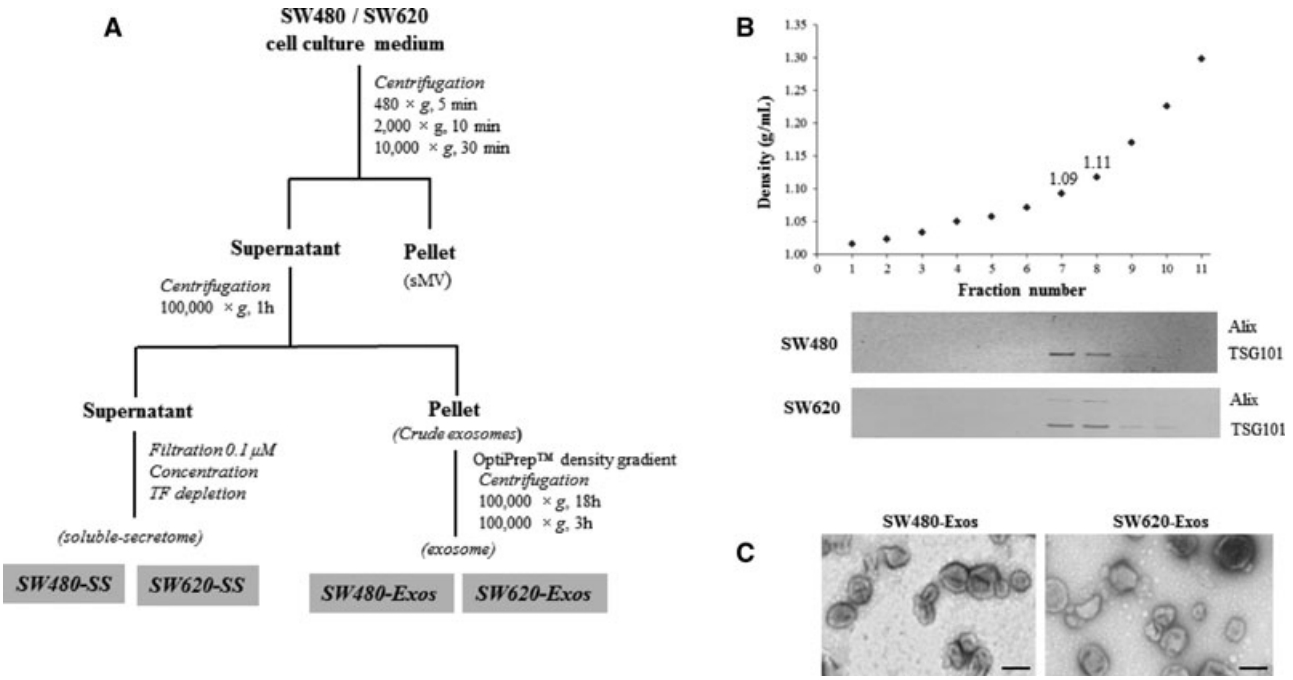

Figure 1. Isolation and characterization of SW480 and SW620 secretome. The experimental workflow used for exosome and soluble-secretome purification (A). SW480 and SW620 cells were grown in RPMI-1640 serum-free medium supplemented with ITS for 24 h, and the CM collected (secretome). sMVs were first isolated from the CM by differential centrifugation. The supernatant was further centrifuged at 100 000 × *g* for 1 h. The supernatant was then filtered (0.1 μm), concentrated by centrifugal ultrafiltration through a 5 K NMWL membrane, and transferrin (TF) depleted using IgY microbeads (soluble-secretome, SS). Following ultracentrifugation, the SW480 and SW620 pellets were fractionated using a 5–40% OptiPrep™ density gradient (100 000 × *g*, 18 h, washed in 1 mL PBS, 100 000 × *g*, 3 h) to obtain purified exosomes (Exos). Following ultracentrifugation, densities of each fraction (11) from the OptiPrep™ density gradient were determined by absorbance at 244 nm using a molar extinction coefficient of 320 L $g^{-1}cm^{-1}$ (B). For Western blotting, each exosome preparation (10 μg) was separated by 1D-SDS-PAGE, electrotransferred, and probed with exosome markers Alix and TSG101 (B). SW480- and SW620-Exos (1.09 g/mL fraction) were negatively stained using uranyl acetate and viewed by electron microscopy (C). Scale bar, 100 nm.

Crude exosomes were purified using OptiPrep™ density gradient as previously described [29]. Briefly, a discontinuous iodixanol gradient was prepared by diluting a stock solution of OptiPrep™ (60% w/v aqueous iodixanol solution with 0.25 M sucrose/10 mM Tris, pH 7.5 to generate 40% w/v, 20% w/v, 10% w/v, and 5% w/v iodixanol solutions). The discontinuous iodixanol gradient was prepared by sequentially adding 3 mL each of 40, 20, and 10% of iodixanol solution to a 14 × 89 mm polyallomer tube (Beckman Coulter) with care. This was followed by layering 2.5 mL of 5% solution. Crude exosomes were resuspended in 500 μL of 0.25 M sucrose/10 mM Tris-HCl, pH 7.5, and loaded onto the top of the gradient. The gradient was centrifuged at 100 000 × *g* for 18 h at 4°C. Eleven individual 1 mL fractions were collected (starting from top of the gradient with increasing density) and each fraction was diluted with 2 mL PBS. After centrifugation at 100 000 × *g* for 3 h at 4°C, the supernatants were discarded and pellets washed with 1 mL PBS and resuspended in 50 μL of PBS. Western blot analysis was used to determine exosome-containing fractions based on the presence of specific exosome markers, Alix and TSG101. The density of each fraction was determined using a control OptiPrep™ gradient loaded with 500 μL of 0.25 M sucrose/10 mM Tris, pH 7.5 run in parallel. Fractions were collected as described, serially diluted 1:10 000 with dH_2O, and iodixanol concentrations were estimated by absorbance at 244 nm using a molar extinction coefficient of 320 L $g^{-1}cm^{-1}$ [30]. The yield of purified exosomes from SW480 (SW480-Exos) and SW620 exosomes (SW620-Exos) was ~15 μg/10^8 cells and ~18 μg/10^8 cells, respectively.

2.4 Electron microscopy (EM)

Exosome samples (1 μg in 10 μL PBS) were applied to 400 mesh carbon-coated copper grids for 2 min. Excess material was removed by blotting, and samples were negatively stained with 10 μL of a 2% uranyl acetate solution for 10 min (ProSciTech, Queensland, Australia). The grids were air dried and viewed using a JEOL JEM-2010 transmission electron microscope operated at 80 kV.

2.5 Cryo-EM and 3D reconstruction

Exosomes obtained from OptiPrep™ gradient fractions were supplemented at 5:1 dilution with colloidal 10-nm gold

particles for tomographic alignment. A 3.5 μL aliquot of mixed suspension was pipetted on a glow-discharged holey carbon-coated EM grid. Excess liquid was blotted and the grid was plunge frozen by rapid immersion in liquid ethane using FEI Vitrobot Mark IV (the Netherlands). Grids containing plunge-frozen samples were mounted on a cryo-holder. Tilt series were recorded at 300 kV on Titan Krios cryo-EM (FEI, the Netherlands) equipped with a Gatan UltraScan4000 (model 895) 16-megapixel CCD. The absolute magnification was ×47 000. Tilt series were collected covering the angular range of –68° ∼ +68° at 2° increments under low-dose conditions, and the total electron dose for each dataset was below 7000 electron/nm^2. Tomographic tilt series were aligned using fiducial markers and tomograms generated using Inspect3D software (FEI, the Netherlands). Surface rendered views were computationally aligned into a 3D reconstructed volume using Amira™ 4.0 (Visage Imaging, Australia).

2.6 SDS-PAGE and Western blotting

SW480 and SW620 cells were lysed in SDS sample buffer with 50 mM DTT and centrifuged at 430 000 × *g* for 30 min to remove insoluble material. The exosome samples were lysed in SDS sample buffer. Both total cellular proteins (30 μg) and exosome proteins (10 μg) were separated by using precast Novex 4–12% Bis–Tris NuPAGE gels with MES running buffer. After electrophoresis, proteins were electrotransferred onto nitrocellulose membranes using the iBlot™ Dry Blotting System (Life Technologies). The membranes were probed with primary antibodies according to manufacturer's instructions. The secondary antibodies (IRDye 800 goat anti-mouse IgG or IRDye 700 goat anti-rabbit IgG) were diluted (1:15 000) and the fluorescent signals were detected using the Odyssey Infrared Imaging System, v3.0 (Li-COR Biosciences, Nebraska, USA).

2.7 Immunoprecipitation

Exosome samples (100 μg per sample) were lysed in 1% TX-100/PBS or 1% Brij 97/PBS containing protease inhibitor cocktail (Roche) for 1 h on ice and centrifuged at 100 000 × *g* for 1 h to remove insoluble material. To reduce nonspecific binding, lysates were preincubated with 50 μL of protein G conjugated Dynabeads for 1 h. After removing the beads, Anti-TNIK antibody (10 μg) was added to the exosome lysates and the mixtures were incubated for 3 h at 4°C. Protein G-Dynabeads (50 μL) was then added and incubated for 1 h at 4°C to isolate the immune complexes. The immune complexes were washed three times with PBS, eluted by using SDS sample buffer and then subjected to SDS-PAGE and Western blotting experiments.

2.8 In vitro proliferation assay

An in vitro proliferation assay based upon reduction of 3-(4,5-dimethylthiazol-2-yl)-2,5-diphenyltetrazolium bromide which corresponds with living cell number and metabolic activity [31]. Briefly, 2F2B cells (3000 cells per well) were cultured for 24 h in a 96-well plate in 100 μL DMEM containing 0.5% w/v BSA and 1% v/v Pen Strep (Life Technologies). CM was supplemented with FCS (10%), PBS or exosomes (0.3, 3, 30 μg/mL) in PBS. Fresh supplements were added at 24 and 48 h. At 72 h, 3-(4,5-dimethylthiazol-2-yl)-2,5-diphenyltetrazolium bromide reagent was added to CM to a final concentration of 50 μg/mL and incubated at 37°C for 4 h. The CM was discarded and cells overlaid with 200 μL acidified isopropanol. Following 1 h incubation at RT under constant shaking, the absorbance of the solution was measured at 560/690 nm.

2.9 GeLC-MS/MS

Density gradient purified exosome samples (30 μg each) were separated using SDS-PAGE and proteins visualized by Imperial protein staining (Pierce). Each gel lane was cut into 30 individual gel bands using a GridCutter (The Gel Company, San Francisco, CA), and gel slices were subjected to reduction, alkylation with iodoacetamide, and tryptic digestion [32]. The extractions containing tryptic peptides from each gel band were concentrated to ∼10 μL by centrifugal lyophilization. RP-HPLC analysis (Model 1200, Agilent) of peptide mixtures was performed on a nanoAcquity (C18) 150 × 0.15-mm id RP-UPLC column (Waters), developed using a linear 60-min gradient from 0 to 100% B (0.1% aqueous formic acid/60% v/v aqueous ACN) with a flow rate of 0.8 μL/min at 45°C and analyzed by LC-MS/MS using an LTQ-Orbitrap mass spectrometer (Thermo Fischer Scientific). Survey MS scans were acquired with resolution set to a value of 30 000. Up to 5 of the most intense ions per cycle were fragmented, and selected ions dynamically excluded for 180s.

2.10 Database searching and protein identification

The parameters used to generate peak lists, using ExtractMSn as part of Bioworks 3.3.1 (Thermo Fisher Scientific), were as follows: minimum mass 700; maximum mass 5000; grouping tolerance 0 Da; intermediate scans 200; minimum group count 1; ten peaks minimum and TIC of 100. Peak lists for each LC-MS/MS run were merged into a single MASCOT generic file. Automatic charge state recognition was used due to the high-resolution survey scan (30 000). LC-MS/MS spectra were searched against the human RefSeq [33] protein database (38 791 sequences) using MASCOT (v2.2.01, Matrix Science, UK). Searching parameters included: fixed modification (carboxymethylation of cysteine; +58 Da), variable modifications (oxidation of methionine;

+16 Da), up to three missed tryptic cleavages, 20 ppm peptide mass tolerance and 0.8 Da fragment ion mass tolerance. Peptide identifications were deemed significant if the ion score was greater than the identity score. Significant protein identifications contained at least two unique peptide identifications. The false-discovery rate (derived from corresponding decoy database search) was less than 0.3% for each sample preparation. The UniProt database was used to classify identified proteins based on their annotated function, subcellular localization, and specify genes reportedly involved in colon cancer [34]. The Human Protein Atlas (www.proteinatlas.org) was used as an annotated resource to assess the tissue expression of proteins identified in this study [35]. To assess protein–protein interactions for TNIK, the STRING database was used (http://string.embl.de) [36].

2.11 Determination of differential protein expression and significance

The fold change ratios of significant spectral count between exosome (Exos) datasets and SS datasets were determined as previously described [29]:

$$\mathrm{Rsc} = (n_{\mathrm{SW620}} + f)(t_{\mathrm{SW480}} - n_{\mathrm{SW480}} + f)/ \times (n_{\mathrm{SW480}} + f)(t_{\mathrm{SW620}} - n_{\mathrm{SW620}} + f) \quad (1)$$

where n is the significant protein spectral count (peptide spectra were considered significant when the Ion score $\geq$ the Homology score), t is the total number of significant spectra in the sample, and f a correction factor set to 1.25 [37]. When Rsc < 1 negative Rsc was used.

3 Results and discussion

3.1 SW480 and SW620 cell line characterization

SW480 and SW620 cells were first grown to 70% confluence and then cell culture was continued in serum-free medium for 24 h to minimize FCS contaminants that would otherwise compromise MS analyses. Under these culture conditions, cell viability for both lines was approximately 95% (assessed by trypan blue staining; data not shown). Cell-based assays were performed to assess cell proliferation, migration, matrix adhesive capacity, anchorage-independent growth, and invasive characteristics. In accordance with previous reports [26, 38–46] our data showed that SW620 cells, when compared with SW480 cells, displayed: a higher proliferation rate, a lower migration rate and matrix adhesive capacity, higher capacity for anchorage-independent growth, and increased invasive capacity (Supporting Information Fig. 1).

3.2 Exosome isolation and characterization

The strategy used in this study for purifying the secretome (exosome and soluble-secretome) of SW480 and SW620 is detailed in Fig. 1A. Intact cells, cell detritus, and large membranous particles were removed from the CM by low-speed centrifugation (480 $\times$ g for 5 min followed by 2000 $\times$ g for 10 min). Ultracentrifugation of the CM was performed at 10 000 $\times$ g for 30 min to isolate sMVs [27]. The supernatant was further centrifuged at 100 000 $\times$ g for 60 min. Soluble-secreted protein (SS fractions) for both SW480 (SW480-SS) and SW620 (SW620-SS) were subsequently isolated following filtration 0.1 μM, ultrafiltration, and immunoaffinity depletion of transferrin from the ITS media. For exosome purification, the crude exosome pellet was resolubilized in PBS (500 μL) and subjected to density gradient fractionation using OptiPrep™ [47]. Ultracentrifugation was performed at 100 000 $\times$ g for 18 h and fractions collected, as described [29]. Western blot analysis revealed that both SW480 (SW480-Exos) and SW620 (SW620-Exos) exosomes were enriched at a buoyant density of 1.09–1.11 g/mL based on expression of stereotypic exosomal markers Alix and TSG101 [29, 48] (Fig. 1B). EM of purified SW480- and SW620-Exos revealed that they were essentially homogeneous 40–100 nm in diameter (Fig. 1C).

3.3 Cryo-electron tomography reveals ultrastructural components within exosomes

To further characterize the morphology of SW480- and SW620-Exos, cryo-electro tomography was performed (see Section 2) (Fig. 2A and B). Tomography showed that these purified exosomes have spherical structure. This is in agreement with a previous reports utilizing cryo-EM to characterize exosomes [49]. In the current study, a total of 68 z-axis sections were computationally constructed into a single tomogram. Interestingly, both SW480- and SW620-Exos tomograms indicate the presence of ultrastructural components, suggestive of large protein complexes (Fig. 2B). This finding is in accord with observed ultrastructural evidence in exosomes secreted by cardiac progenitor cells [50].

3.4 Proteomic analysis of the SW480 and SW620 secretome

We next compared the proteome profiles of the secretome (exosomes and soluble secreted) from SW480 and SW620 cells using GeLC-MS/MS [27, 29]. For purified exosomes, this resulted in 941 and 796 proteins identified in SW480- and SW620-Exos, respectively (Fig. 3A) (Supporting Information Table 1). Six hundred twenty-eight proteins were identified in common including typical exosome protein markers such as ESCRT components TSG101, various VPS3 and CHMP components, Alix, and tetraspanins CD9 and

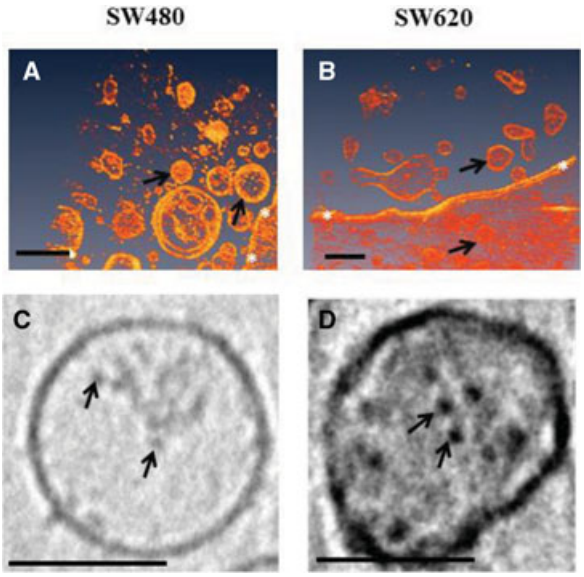

Figure 2. Tomography of SW480- and SW620-Exos purified using OptiPrep™ gradient. Isosurface 3D reconstruction of exosomes show both SW480 (A) and SW620 (B) contain vesicles sized from 40–130 nm (arrows) (scale 100 nm). The edges of carbon-coated copper grids are indicated by white asterisks (*). Dense ultrastructural components (arrows) are observed within both SW480 (C) and SW620 (D) exosomes (scale 50 nm).

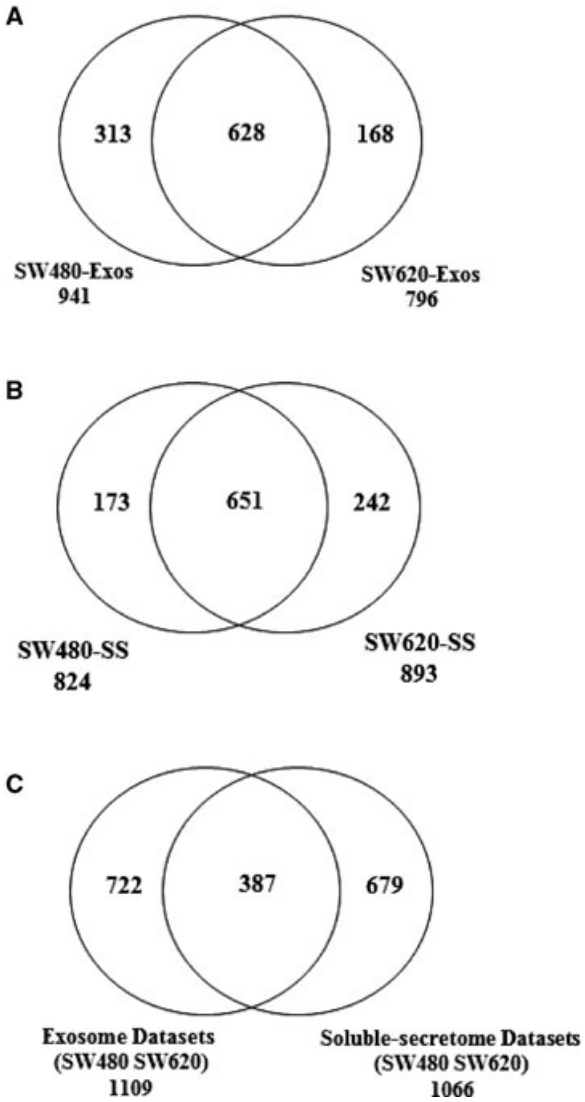

Figure 3. Secretome protein identification and subcellular localization. A two-way Venn of SW480- and SW620-Exos reveals 628 proteins were commonly identified, while 313 and 168 proteins were uniquely identified in SW480- and SW620-Exos, respectively (A). A comparison between SW480- and SW620-SS reveals 651 proteins were commonly identified, while 173 and 242 proteins were uniquely identified in SW480- and SW620-SS, respectively (B). Comparison between exosome and soluble-secretome protein identifications from SW480 and SW620 cell lines, indicates 387 proteins in common between exosome and SS datasets (C).

CD63 (Supporting Information Table 2). Both 313 and 168 proteins were uniquely identified in SW480- and SW620-Exos datasets, respectively (Fig. 3A). A detailed list of proteins identified in our SW480- and SW620-Exos datasets, along with earlier reports [51] is given in Supporting Information Table 1—this table also lists 384 proteins not previously described for SW480- and SW620-Exos based on proteomic comparison with Choi et al. [51] including tetraspanin CD63, claudins 3, 4, and 7, ADP-ribosylation factor 1 (ARF1), and various Rab members (RAB1B, RAB2B, RAB3A, RAB3B, RAB3D, RAC3C, RAB5B, RAB6B, RAB6C, RAB11, RAB15, and RAB43). Proteins associated with exosome biogenesis, organization, and sorting of vesicular trafficking including Rab GTPases, ADP-ribosylation factors, syntenins, and components involved in recognition and uptake (VAMPs, LAMPs, syntaxins) [52, 53] are shown in Supporting Information Table 2. To validate the relative abundance of proteins using GeLC-MS/MS (relative spectral count ratios (Rsc) [29], see Materials and methods), Western blot analysis was performed for selected proteins; v-src (SRC), flotillin 1 (FLOT1), transferrin receptor, CD9, HSP70, EGFR, Alix, and TSG101 (Fig. 4), revealing similar protein expression differences between exosome datasets.

To further assess the contribution of the SW480 and SW620 secretome in the context of the tumor microenvironment, we analyzed proteome profiles of the soluble-secretome from SW480 (SW480-SS) and SW620 (SW620-SS) cells using GeLC-MS/MS (Section 2.3). This study identified 824 and 893 proteins in SW480- and SW620-SS, respectively, of which 651 were in common between both datasets (Fig. 3B) (Supporting Information Table 3). When SW480- and SW620-SS were compared with the SW480- and SW620-Exos, 387 proteins were found to be common, including various secreted (e.g. tenascin, fibronectin, urokinase-type plasminogen activator), and membrane-spanning proteins (e.g. ephrin-B2, MET receptor, and cell surface glycoprotein MUC18) (Fig. 3C) (Supporting Information Table 3).

Table 1. Secretome of SW480 and SW620 contain components shown to modulate tumor and metastatic environment

Gene symbol	Gene ID	Protein description	SW480-Exos SpC[a)]	SW620-Exos SpC[b)]	Exosome R_{SC} (SW620-Exos/ SW480-Exos)[c)]	Soluble-secreted R_{SC} (SW620-SS/ SW480-SS)[d)]
TNC	3371	Tenascin C		33	37.8	29.5
CLDN1	9076	Claudin 1		23	26.7	
SRC	6714	v-src sarcoma		18	21.2	
PROM1	8842	Prominin 1		17	20.1	
EFNB2	1948	Ephrin-B2		13	15.7	4.4
S100A14	57 402	S100 calcium binding protein A14		13	15.7	
MET	4233	Met proto-oncogene (hepatocyte growth factor receptor)		9	11.3	16.2
S100A9	6280	S100 calcium binding protein A9		6	8.0	
GLG1	2734	Golgi apparatus protein 1		5	6.9	10.6
ADAM9	8754	ADAM metallopeptidase domain 9		4	5.8	
S100A8	6279	S100 calcium binding protein A8		4	5.8	
PTPRK	5796	Protein tyrosine phosphatase, receptor type, K		3	4.7	2.0
STUB1	10 273	STIP1 homology and U-box containing protein 1		3	4.7	
ITGA5	3678	Integrin, alpha 5	10	29	3.7	
ITGA7	3679	Integrin, alpha 7		2	3.6	
ADAM10	102	ADAM metallopeptidase domain 10	10	19	2.5	
ITGA2	3673	Integrin, alpha 2	41	69	2.3	
ITGB4	3691	Integrin, beta 4	232	291	1.7	
ARHGDIA	396	Rho GDP dissociation inhibitor (GDI) alpha	5	6	1.6	1.7
RPLP2	6181	Ribosomal protein, large, P2	12	10	1.2	−1.7
S100A6	6277	S100 calcium binding protein A6	14	10	1.0	1.5
S100A4	6275	S100 calcium binding protein A4	11	4	−1.7	−1.0
MMP14	4323	Matrix metallopeptidase 14 (membrane-inserted)	6		−4.2	
CD44	960	CD44 molecule (Indian blood group)	57		−33.9	
EGFR	1956	Epidermal growth factor receptor	60		−35.7	

a) Significant MS/MS spectral counts identified in SW480-Exos.
b) Significant MS/MS spectral counts identified in SW620-Exos.
c) Relative spectral count ratio (Rsc) for proteins identified in SW480-Exos, compared with SW620-Exos (Eq. 1).
d) Relative spectral count ratio (Rsc) for proteins identified in SW480-SS, compared with SW620-SS (Eq. 1).

Subcellular localization and protein function of SW480 and SW620 (Exos and SS) based on Gene Ontology annotation [54, 55] is shown in Supporting Information Figs. 3 and 4. Based on subcellular localization, increased levels of cell membrane proteins in Exos were observed in comparison to SS, while increased levels of secreted proteins were observed in SS in comparison to Exos.

3.5 Secretome contains components known to modulate metastatic niche and tumor progression

Tumor-derived secretomes have been reported to have the ability to facilitate tumor growth and metastasis [11, 56, 57]. To gain insights into the role of the CRC secretome throughout the metastatic environment, we compared our data with several key studies investigating metastatic factors that modulate the metastatic niche [1, 6, 10, 56–60]. Several mediators of tissue invasion, intravasation, and metastasis identified in this study including growth factor receptors, components throughout the extracellular matrix (ECM), and chemoattractants are included in Table 1.

Hepatocyte growth factor receptor tyrosine kinase Met (MET) (Exos: Rsc 11.3, SS: Rsc 16.2) is a protein important in regulating proliferation, motility, mitogenesis, and morphogenesis. The MET proto-oncogene, which is expressed in both stem and cancer cells, is a key regulator of cancer progression and metastasis [12,61]. Increased expression of MET is frequently observed in various human tumors, including colorectal carcinomas [62], and associated with a metastatic phenotype and poor prognosis. Further, MET signaling is a potent inducer of endothelial cell growth and promotes angiogenesis and lymphangiogenesis in vitro and in vivo [63, 64]. Functional crosstalk of MET with various components including EGFR has been reported [65] to modulate key signaling pathways, such as Wnt–β-catenin and TGFβ–bone morphogenetic protein systems. In the context of the secretome, CM

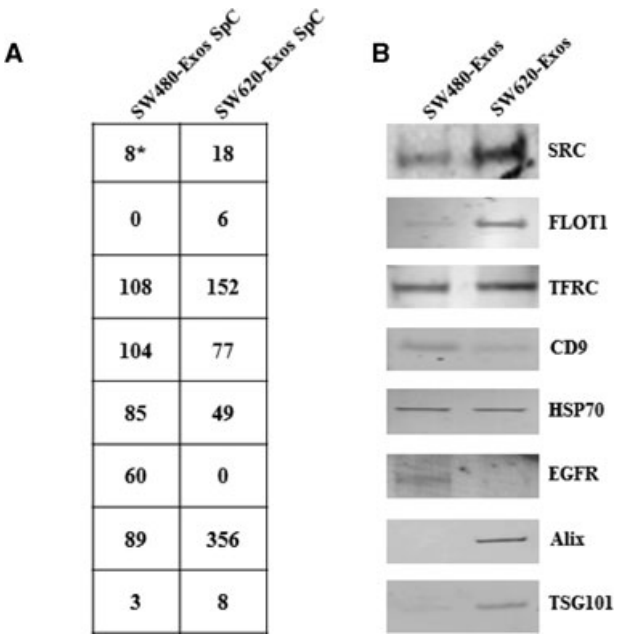

Figure 4. Comparison of relative quantitation of mass spectrometry and Western blot analyses. For SW480- and SW620-Exos, relative spectral count ratios (Rsc) were determined as detailed in Eq. 1 (A). To validate the relative abundance of proteins using GeLC-MS/MS, Western blot analysis was compared for selected proteins; v-src (SRC), flotillin 1 (FLOT1), transferrin receptor (TFRC), CD9, HSP70, EGFR, Alix, and TSG101. For Western blotting, exosomes (10 μg) were separated by 1D-SDS-PAGE, electrotransferred, and probed with markers as indicated (B). *For Src, only a single significant peptide was identified (eight unique spectral counts). The peptide was manually validated and the MASCOT MS/MS profile for the peptide "LIEDNEYTAR" is shown in Supporting Information Fig. 2.

from human tumor cells in vitro has been recently shown to induce elevated production of the MET ligand, HGF [66]. This suggests that tumor cells secrete factors that induce HGF secretion, which in turn activates MET in a paracrine fashion to induce tumor cell invasiveness through the surrounding stroma. Recently, Peinado et al. have demonstrated that transfer of several key oncoproteins including MET from tumor-derived exosomes to bone marrow progenitor cells promotes the metastatic process in vivo [12].

Tenascin C (TNC) (Exos: Rsc 37.8, SS: Rsc 29.5) is an extracellular matrix protein, associated with remodeling and deposition of the ECM and formation of the metastatic niche. TNC has recently been shown from primary breast cancer cells to colonize lung metastatic niche formation [59, 67]. It has been suggested that TNC may promote tumor cell dissemination and survival during metastasis by binding growth factors, and reciprocal interactions with ECM components such as fibronectin, proteoglycans, and fibrinogen, enzymes such as matrix metalloproteinases, and cell surface receptors including EGFR and integrins [68]. Ephrin-B2 (EFNB2) (Exos: Rsc 15.7, SS: Rsc 4.4), a transmembrane ligand for Eph receptors, is important in mediating cell migration and vascular architecture [69]. Deregulation of EFNB2 expression has been linked to tumor progression and is suggested to play a role in cancer progression and metastasis [70]. Further, EFNB2 is expressed at higher levels in human CRC than in adjacent normal mucosa [71], and attributed with development of dysfunctional vascular in an in vivo CRC model [72]. Recently, upregulation of the EPHB4 in exosomes has been suggested a mechanism whereby priming of the lymph node metastatic environment supports colocalization [9]. EPHB4 receptor has been shown to promote proliferation and survival of melanoma cells expressing EFNB2 in vivo, in addition to angiogenesis [73].

Claudin 1 (CLDN1) (Exos: Rsc 26.7) was shown to be upregulated in SW620-Exos. Claudins are members of the tight junction family, associated with actin cytoskeleton remodeling and have been shown to be dysregulated in various human cancers, including CRC [74]. CLDN1 expression has been highlighted in human primary colon carcinoma and metastasis, and shown to significantly modulate xenograft liver metastasis in vivo [75]. Further, the chemoattractant S100 calcium-binding proteins S100A8 (Exos: Rsc 5.8) and S100A9 (Exos: Rsc 8.0) were identified upregulated in SW620-Exos. S100 proteins are commonly upregulated in tumors and often associated with tumor progression, including CRC [76,77]. S100A8 and S100A9 facilitate the homing of tumor cells to premetastatic sites within the lung parenchyma. Recently, primary lung tumors were shown to secrete soluble factors, including VEGF-A, TGF-β, and TNF-α, capable of inducing expression of S100A8 and S100A9 prior to tumor metastasis [78]. Although it is evident that specific cell adhesion components, receptors, and chemoattractants are key regulators of the tumor microenvironment and metastasis, the role of the secretome—specifically exosome components—in this environment remains to be investigated in the context of CRC progression and metastasis.

3.6 Key signaling molecules MET and TNIK identified in exosomes

Key signaling components and binding partners associated with tumor progression were identified in our exosome datasets. Of note were MET (Exos: Rsc 11.3), and TRAF2 and NCK interacting kinase (TNIK) (Exos: Rsc 8.5) (Table 2).

MET—Tumor-derived exosomes have been reported to facilitate tumor growth and metastasis [79]. As discussed, melanoma-derived exosomes have been demonstrated, through a MET signaling-dependent pathway, to promote the metastatic process in vivo [12]. Exosomes from metastatic melanomas containing activated MET increased metastatic behavior of primary tumors promoting the education and mobilization of bone marrow progenitor cells. Upon activation, various cytoplasmic effector molecules including growth factor receptor-bound protein 2 (GRB2),

Table 2. Differentially expressed proteins associated with MET, TNIK, and EpCAM in SW480- and SW620-Exos

	Gene symbol	Gene ID	Protein description	SW480-Exos SpC[a)]	SW620-Exos SpC[b)]	R_{SC} (SW620-Exos/SW480-Exos)[c)]
MET protein complex	MET	4233	Met proto-oncogene (hepatocyte growth factor receptor)		9	11.3
	SRC	6714	v-src sarcoma		18	21.2
	GRB2	2885	Growth factor receptor-bound protein 2		8	10.2
TNIK protein complex	TNIK	23043	TRAF2 and NCK interacting kinase	3	25	8.5
	RAP2A	5911	RAP2A, member of RAS oncogene family		37	42.2
	CTNNB1	1499	Catenin (cadherin-associated protein), beta 1	87	95	1.5
EpCAM protein complex	EPCAM	4072	Epithelial cell adhesion molecule	150	70	−1.5
	CDH1	999	Cadherin 1, type 1, E-cadherin	2	22	9.9
	CD44	960	CD44 molecule	57		−33.9
	CLDN7	1366	Claudin 7	23		−14.1

a) Significant MS/MS spectral counts identified in SW480-Exos.
b) Significant MS/MS spectral counts identified in SW620-Exos.
c) Relative spectral count ratio (Rsc) for proteins identified in SW480-Exos, compared with SW620-Exos (Eq. 1).

GRB2-associated-binding protein 1, phospholipase C and SRC are further recruited to the MET receptor [61]. In this study, we report the identification of GRB2 (Exos: Rsc 10.2) and SRC (Exos: Rsc 21.2), both unique to SW620-Exos. Whether these proteins in this study associate to form a complex in the context of the tumor microenvironment and subsequently modulate the metastatic niche during CRC remains to be investigated.

TNIK—The Wnt signaling pathway is involved in differentiation during embryonic development and through

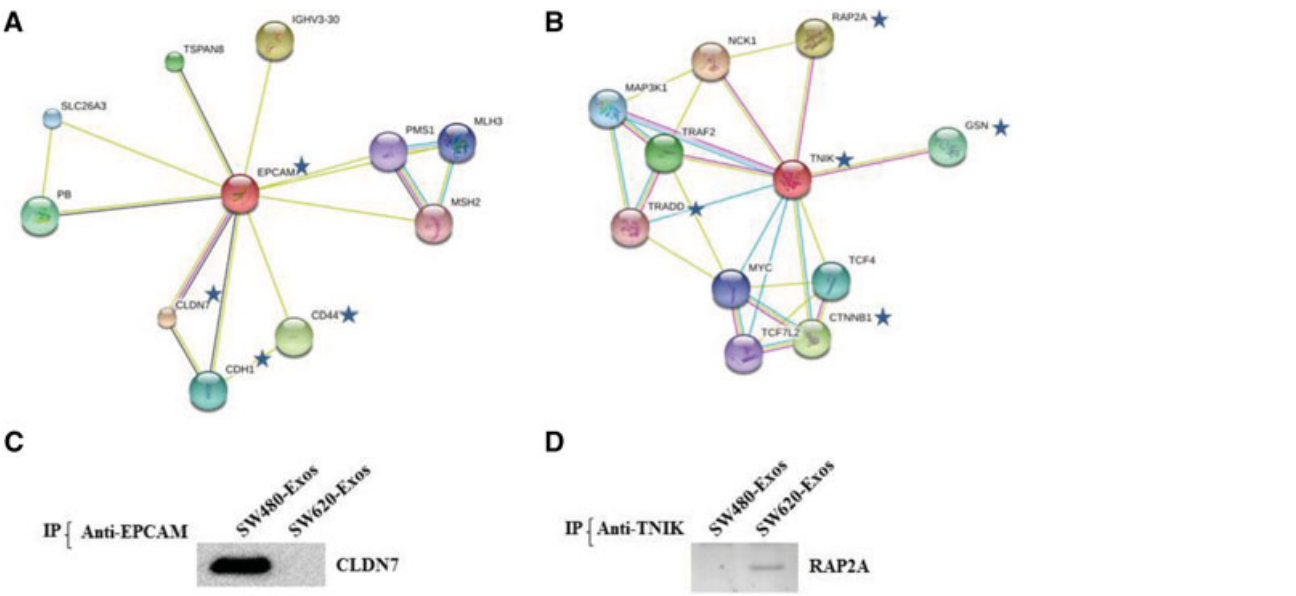

Figure 5. Detection of protein complexes EpCAM-Claudin-7 and TNIK-RAP2A in exosomes. Protein interaction network shown by STRING analysis reveals several components identified in this study to interact with EpCAM and TNIK shown by blue stars. Identified components shown to interact with EpCAM include CLDN7, CD44, and CDH1 (A), while identified components shown to interact with TNIK include RAP2A, GSN, and CTNNB1 (B). For immunoprecipitation (IP), 100 μg of SW480- and SW620-Exos were lysed in either 1% Brij 97 for anti-EpCAM (C), or 1% TX-100 for anti-TNIK (D). Western blotting showed anti-CLDN7 associated with EPCAM in SW480-Exos, while anti-RAP2A was shown to associate with TNIK in SW620-Exos.

Table 3. Selected proteins identified in SW480- and SW620-Exos

	Gene symbol	Gene ID	Protein description	SW480-Exos SpC[a)]	SW620-Exos SpC[b)]	R_{SC} (SW620-Exos/SW480-Exos)[c)]
Lipid raft formation	CAV1	857	Caveolin 1, caveolae protein, 22kDa		8	10.2
	FLOT1	10211	Flotillin 1		6	8.0
	FLOT2	2319	Flotillin 2		2	3.6
Src signaling/ endocytosis/ caveolae formation	SRC	6714	v-src sarcoma		18	21.2
	HCK	3055	Hemopoietic cell kinase		8	10.2
	FGR	2268	Gardner-Rasheed feline sarcoma viral		7	9.1
	LCK	3932	Lymphocyte-specific protein tyrosine kinase	10	38	4.8
	LYN	4067	v-yes-1 Yamaguchi sarcoma viral related oncogene homolog	3	10	3.6
	FYN	2534	FYN oncogene related to SRC, FGR, YES	13	31	3.1
Stem cell marker	PROM1	8842	Prominin 1		17	20.1
	CD44	960	CD44 molecule (Indian blood group)	57		−33.9
Cytoskeletal remodeling	VIL1	7429	Villin 1		15	17.9
	ADAM10	102	ADAM metallopeptidase domain 10	10	19	2.5
	CD9	928	CD9 molecule	104	77	1.0
	EZR	7430	Ezrin	192	87	−1.6
	ANXA2	302	Annexin A2	263	84	−2.3
Signaling	KRAS	3845	v-Ki-ras2 Kirsten rat sarcoma viral oncogene	4	17	4.8
	HRAS	3265	v-Ha-ras Harvey rat sarcoma viral oncogene	5	15	3.6
	NRAS	4893	Neuroblastoma RAS viral (v-ras) oncogene	5	12	2.9
	RRAS2	22800	Related RAS viral (r-ras) oncogene homolog 2	13	18	1.9
	RRAS	6237	Related RAS viral (r-ras) oncogene homolog	11	13	1.6
	CD81	975	CD81 molecule	56	48	1.2
Membrane modification	MYOF	26509	Myoferlin	4	240	63.8
	ANXA4	307	Annexin A4	9	18	2.6

a) Significant MS/MS spectral counts identified in SW480-Exos.
b) Significant MS/MS spectral counts identified in SW620-Exos.
c) Relative spectral count ratio (Rsc) for proteins identified in SW480-Exos, compared with SW620-Exos (Eq. 1).

activating mutations of the TCF4/β-catenin transcriptional program, leads to tumorigenesis [80]. β-Catenin, a cytoplasmic component, plays a major role in the transduction of canonical Wnt signaling. TNIK is a serine/threonine kinase that is an essential activator of Wnt signaling [81]. It is recruited to promoters of Wnt target genes to activate their expression in a β-catenin-dependent manner [81]. Furthermore, TNIK forms a complex with RAP2A to regulate cytoskeletal rearrangement by disrupting F-actin and cell spreading [82]. The same protein complex also functions in regulating neuronal dendrite extension during development [83]. Interestingly, in the context of colon biology, Rap2A and its effector TNIK, have recently been shown to be involved in intestinal cell polarity and brush border formation [84]. In this study, we report the identification of RAP2A (Exos: Rsc 42.2) unique to the SW620-Exos dataset.

3.7 Protein complexes identified in SW480- and SW620-Exos

To investigate protein–protein interactions within SW480- and SW620-Exos, the STRING database was utilized [36]. These analyses revealed several interacting components with EPCAM (Fig. 5A), including CD44 (Exos: Rsc –33.9), CDH1 (Exos: Rsc 9.9), and CLDN7 (Exos: Rsc –14.1), and interacting proteins with TNIK (Fig. 5B) including β-catenin (CTNNB1) (Exos: Rsc 1.5) and RAP2A (Exos: Rsc 42.2) (Table 2). Known

interacting protein partners of EpCAM and TNIK were examined using IP and Western blotting for their ability to associate as protein complexes within exosomes. To examine the presence of the EPCAM-CLDN7 protein–protein interaction in exosomes, we performed IP with anti-EpCAM antibody and WB analysis using anti-Claudin-7 (Fig. 5C). To assess the theTNIK-RAP2A protein–protein interaction in exosomes, we performed IP with anti-TNIK and subsequent WB analysis using anti-RAP2A (Fig. 5D). Based on co-IP EPCAM-CLDN7 and TNIK-RAP2A are shown to complex in SW480- and SW620-Exos, respectively (Fig. 5C and D). The EPCAM-CLDN7 complex has been reported to strongly promote tumorigenicity, accelerate tumor growth, and support ascites production and thymic metastasis formation [85]. To our knowledge, this is the first experimental evidence showing the presence of a TNIK-associated protein complex in exosomes. Further experiments are required to explore how the TNIK protein complex is enriched in exosomes and if this protein complex regulates cytoskeleton remodeling during exosome biogenesis and trafficking.

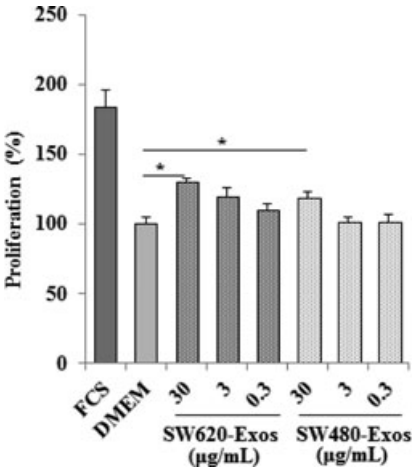

Figure 6. Exosomes induce endothelial cell proliferation. A 3-(4,5-dimethylthiazol-2-yl)-2,5-diphenyltetrazolium bromide cell proliferation assay [31] of 2F2B cells stimulated with SW480- and SW620-Exos at varying concentrations (0.3–30 μg/mL). *$p < 0.05$, $n = 3$ biological replicates.

3.8 Enrichment of lipid raft and lipid raft-associated proteins in SW620 exosomes

Lipid raft membrane microdomains are cholesterol-enriched membrane microdomains that function as selective regions for signal transduction [86] and are implicated in modulating the malignant phenotype of cancer [87]. We next compared our SW480- and SW620-Exos datasets with previous proteomic studies that focused on cellular [88], plasma membrane and exosomal [24, 89–91] lipid raft constituents (Supporting Information Table 3). Proteins shown to function in lipid raft formation and scaffold (FLOT1 Rsc 8.0, FLOT2 Rsc 3.6, CAV1 Rsc 10.2), cytoskeletal remodeling (VIL1 Rsc 17.9), signal transduction (HRAS Rsc 3.6, KRAS Rsc 4.8, NRAS Rsc 2.9, PROM1 Rsc 20.1), and membrane modifications (MYOF Rsc 63.8) [89] were significantly enriched in SW620 exosomes (Table 3). Recently, FLOT1 and FLOT2 were shown to promote coassembly of activated GPI-anchored proteins in lipid rafts and enable the interaction of signaling molecules, such as Src family kinases to coordinate downstream signaling [92]. CAV1 has been demonstrated to interact with G proteins, adenylate cyclase isoforms and a series of tyrosine kinases such as Src family kinases, MAPK, protein kinase (PK) A, and PKC) [93]. Various Src family kinases were also enriched in SW620-Exos, including Src (Rsc 21.2), Lyn (Rsc 3.6), and Fyn (Rsc 3.1). Interactions between CAV1, FLOT1, and FLOT2 with Src kinases are involved in signal transduction, endocytosis and cytoskeleton remodeling [92]. The pentaspan glycoprotein PROM1 has been associated with tumor progression in lung, pancreatic, liver, prostate, gastric, colorectal, and head and neck cancers [94–97]. PROM1 has been identified in exosomes in several recent studies [98–100]. In human metastatic melanoma PROM1 has been shown to influence cell growth and cell motility [101]. Enrichment of lipid raft and lipid raft-associated components in SW620 exosomes suggests roles in signal transduction and mediating intercellular communication. Interestingly, enrichment of lipid rafts has been implicated in modulating various signaling pathways to promote cell transformation and tumor progression [102].

3.9 SW480- and SW620-Exos promote proliferation of endothelial cells in vitro

To demonstrate that SW480- and SW620-Exos transport functionally active cargo, exosomes were investigated for their ability to assist proliferation of mouse endothelial 2F2B cells. 2F2B cells cultured in DMEM-supplemented with SW480- or SW620-Exos in a dose-dependent manner, displayed higher proliferation rates compared with DMEM alone (Fig. 6). Interestingly, addition of 30 μg/mL SW480- or SW620-Exos were shown to significantly increase cell proliferation in 2F2B cells in comparison to DMEM ($p < 0.05$). No significant change in cell proliferation was observed between SW480- and SW620-Exos. Tumor exosomes (30 μg/mL) derived from BT-474 cells have been shown to slightly, but significantly increase cell proliferation of BT-474 cells [103]. Further, gastric cancer SGC7901-cell-derived exosomes have been shown to promote activation of PI3K/Akt and proliferation of SGC7901 and BGC823 cells [104].

4 Concluding remarks

In this study, secretome protein profiles released in vitro from isogenic human colorectal cancer cells SW480 and SW620

were analyzed by GeLC-MS/MS and shown to contain known secreted modulators of the metastatic niche. To our knowledge, this is the first demonstration of selective enrichment of key metastatic factors (MET, S100A8, S100A9, TNC) and signal transduction molecules (EFNB2, EGFR, JAG1, SRC, TNIK) in metastatic CRC cell exosomes relative to primary CRC cell exosomes. Additionally, Met signal transduction components, Met, Src, and GRB2 were uniquely expressed in SW620-Exos. Importantly, the TNIK-RAP2A complex, a key regulator of cytoskeletal rearrangement and cell spreading, was uniquely identified in SW620-Exos. Significant enrichment of several lipid raft and lipid raft-associated components was also observed in SW620-Exos. Given that many of the proteins selectively enriched in metastatic CRC cell-derived exosomes can act both as metastatic factors and in important signaling pathways, elucidation of the function of these exosomes in the tumor microenvironment will extend our understanding of tumor progression with potential impact on our understanding of cross-talk between stromal cells and design of targeted CRC therapeutics.

This work was supported by the National Health & Medical Research Council of Australia (NH&MRC) program grant #487922 (R.J.S., D.W.G., J.H.). B.J.T. is supported by a University of Melbourne Research Scholarship. S.M. was supported by a NH&MRC Fellowship #1016599. Analysis of proteomic data described in this work was supported by the Australian Proteomics Computational Facility funded by the NH&MRC grant #381413. This work was supported by funds from the Operational Infrastructure Support Program provided by the Victorian Government Australia. We acknowledge the Australian Cancer Research Foundation for providing funds to purchase the Orbitrap™ mass spectrometer.

The authors have declared no conflict of interest.

5 References

[1] Joyce, J. A., Pollard, J. W., Microenvironmental regulation of metastasis. *Nat. Rev. Cancer* 2009, *9*, 239–252.

[2] Mbeunkui, F., Johann, D. J., Jr., Cancer and the tumor microenvironment: a review of an essential relationship. *Cancer Chemother. Pharmacol.* 2009, *63*, 571–582.

[3] Albini, A., Sporn, M. B., The tumour microenvironment as a target for chemoprevention. *Nat. Rev. Cancer* 2007, *7*, 139–147.

[4] Kenny, P. A., Lee, G. Y., Bissell, M. J., Targeting the tumor microenvironment. *Frontiers Biosci.* 2007, *12*, 3468–3474.

[5] Dvorak, H. F., Weaver, V. M., Tlsty, T. D., Bergers, G., Tumor microenvironment and progression. *J. Surg. Oncol.* 2011, *103*, 468–474.

[6] Psaila, B., Lyden, D., The metastatic niche: adapting the foreign soil. *Nat. Rev. Cancer* 2009, *9*, 285–293.

[7] Simpson, R. J., Lim, J. W., Moritz, R. L., Mathivanan, S., Exosomes: proteomic insights and diagnostic potential. *Expert Rev. Proteomics* 2009, *6*, 267–283.

[8] Thery, C., Exosomes: secreted vesicles and intercellular communications. *F1000 Biol. Rep.* 2011, *3*, 15.

[9] Hood, J. L., San, R. S., Wickline, S. A., Exosomes released by melanoma cells prepare sentinel lymph nodes for tumor metastasis. *Cancer Res.* 2011, *71*, 3792–3801.

[10] Jung, T., Castellana, D., Klingbeil, P., Cuesta Hernandez, I. et al., CD44v6 dependence of premetastatic niche preparation by exosomes. *Neoplasia* 2009, *11*, 1093–1105.

[11] Peinado, H., Lavotshkin, S., Lyden, D., The secreted factors responsible for pre-metastatic niche formation: old sayings and new thoughts. *Semin. Cancer Biol.* 2011, *21*, 139–146.

[12] Peinado, H., Aleckovic, M., Lavotshkin, S., Matei, I. et al., Melanoma exosomes educate bone marrow progenitor cells toward a pro-metastatic phenotype through MET. *Nat. Med.* 2012, *18*, 883–891.

[13] Mathivanan, S., Ji, H., Simpson, R. J., Exosomes: extracellular organelles important in intercellular communication. *J. Proteomics* 2010, *73*, 1907–1920.

[14] Thery, C., Zitvogel, L., Amigorena, S., Exosomes: composition, biogenesis and function. *Nat. Rev. Immunol.* 2002, *2*, 569–579.

[15] Higginbotham, J. N., Demory Beckler, M., Gephart, J. D., Franklin, J. L. et al., Amphiregulin exosomes increase cancer cell invasion. *Curr. Biol.* 2011, *21*, 779–786.

[16] Sheldon, H., Heikamp, E., Turley, H., Dragovic, R. et al., New mechanism for Notch signaling to endothelium at a distance by Delta-like 4 incorporation into exosomes. *Blood* 2010, *116*, 2385–2394.

[17] Putz, U., Howitt, J., Doan, A., Goh, C. P. et al., The tumor suppressor PTEN is exported in exosomes and has phosphatase activity in recipient cells. *Sci. Signal.* 2012, *5*, ra70.

[18] Rak, J., Guha, A., Extracellular vesicles–vehicles that spread cancer genes. *Bioessays* 2012, *34*, 489–497.

[19] Record, M., Subra, C., Silvente-Poirot, S., Poirot, M., Exosomes as intercellular signalosomes and pharmacological effectors. *Biochem. Pharmacol.* 2011, *81*, 1171–1182.

[20] Skog, J., Wurdinger, T., van Rijn, S., Meijer, D. H. et al., Glioblastoma microvesicles transport RNA and proteins that promote tumour growth and provide diagnostic biomarkers. *Nat. Cell. Biol.* 2008, *10*, 1470–1476.

[21] Valadi, H., Ekstrom, K., Bossios, A., Sjostrand, M. et al., Exosome-mediated transfer of mRNAs and microRNAs is a novel mechanism of genetic exchange between cells. *Nat. Cell Biol.* 2007, *9*, 654–659.

[22] Umezu, T., Ohyashiki, K., Kuroda, M., Ohyashiki, J. H., Leukemia cell to endothelial cell communication via exosomal miRNAs. *Oncogene* 2012, doi:10.1038/onc.2012.295.

[23] de Gassart, A., Geminard, C., Fevrier, B., Raposo, G., Vidal, M., Lipid raft-associated protein sorting in exosomes. *Blood* 2003, *102*, 4336–4344.

[24] Staubach, S., Razawi, H., Hanisch, F. G., Proteomics of MUC1-containing lipid rafts from plasma membranes and exosomes of human breast carcinoma cells MCF-7. *Proteomics* 2009, *9*, 2820–2835.

[25] Rana, S., Zoller, M., Exosome target cell selection and the importance of exosomal tetraspanins: a hypothesis. *Biochem. Soc. Trans.* 2011, *39*, 559–562.

[26] Leibovitz, A., Stinson, J. C., McCombs, W. B., 3rd, McCoy, C. E. et al., Classification of human colorectal adenocarcinoma cell lines. *Cancer Res.* 1976, *36*, 4562–4569.

[27] Tauro, B. J., Greening, D. W., Mathias, R. A., Mathivanan, S. et al., Two distinct populations of exosomes are released from LIM1863 colon carcinoma cell-derived organoids. *Mol. Cell. Proteomics*. 2012, *12*, 587–598.

[28] Ji, H., Greening, D. W., Kapp, E. A., Moritz, R. L., Simpson, R. J., Secretome-based proteomics reveals sulindac-modulated proteins released from colon cancer cells. *Proteomics Clin. Appl.* 2009, *3*, 433–451.

[29] Tauro, B. J., Greening, D. W., Mathias, R. A., Ji, H. et al., Comparison of ultracentrifugation, density gradient separation, and immunoaffinity capture methods for isolating human colon cancer cell line LIM1863-derived exosomes. *Methods* 2012, *56*, 293–304.

[30] Schroder, M., Schafer, R., Friedl, P., Spectrophotometric determination of iodixanol in subcellular fractions of mammalian cells. *Anal. Biochem.* 1997, *244*, 174–176.

[31] Ji, H., Moritz, R. L., Kim, Y. S., Zhu, H. J., Simpson, R. J., Analysis of Ras-induced oncogenic transformation of NIH-3T3 cells using differential-display 2-DE proteomics. *Electrophoresis* 2007, *28*, 1997–2008.

[32] Simpson, R. J., Connolly, L. M., Eddes, J. S., Pereira, J. J. et al., Proteomic analysis of the human colon carcinoma cell line (LIM 1215): development of a membrane protein database. *Electrophoresis* 2000, *21*, 1707–1732.

[33] Pruitt, K. D., Tatusova, T., Maglott, D. R., NCBI reference sequences (RefSeq): a curated non-redundant sequence database of genomes, transcripts and proteins. *Nucleic. Acids. Res.* 2007, *35*, D61–65.

[34] Apweiler, R., Bairoch, A., Wu, C. H., Barker, W. C. et al., UniProt: the Universal Protein knowledgebase. *Nucleic Acids Res.* 2004, *32*, D115–119.

[35] Uhlen, M., Bjorling, E., Agaton, C., Szigyarto, C. A. et al., A human protein atlas for normal and cancer tissues based on antibody proteomics. *Mol. Cell. Proteomics* 2005, *4*, 1920–1932.

[36] Szklarczyk, D., Franceschini, A., Kuhn, M., Simonovic, M. et al., The STRING database in 2011: functional interaction networks of proteins, globally integrated and scored. *Nucleic Acids Res.* 2011, *39*, D561–568.

[37] Old, W. M., Meyer-Arendt, K., Aveline-Wolf, L., Pierce, K. G. et al., Comparison of label-free methods for quantifying human proteins by shotgun proteomics. *Mol. Cell Proteomics* 2005, *4*, 1487–1502.

[38] Hewitt, R. E., Brown, K. E., Corcoran, M., Stetler-Stevenson, W. G., Increased expression of tissue inhibitor of metalloproteinases type 1 (TIMP-1) in a more tumourigenic colon cancer cell line. *J. Pathol.* 2000, *192*, 455–459.

[39] Hewitt, R. E., McMarlin, A., Kleiner, D., Wersto, R. et al., Validation of a model of colon cancer progression. *J. Pathol.* 2000, *192*, 446–454.

[40] Huerta, S., Harris, D. M., Jazirehi, A., Bonavida, B. et al., Gene expression profile of metastatic colon cancer cells resistant to cisplatin-induced apoptosis. *Int. J. Oncol.* 2003, *22*, 663–670.

[41] Huerta, S., Heinzerling, J. H., Anguiano-Hernandez, Y. M., Huerta-Yepez, S. et al., Modification of gene products involved in resistance to apoptosis in metastatic colon cancer cells: roles of Fas, Apaf-1, NFkappaB, IAPs, Smac/DIABLO, and AIF. *J. Surg. Res.* 2007, *142*, 184–194.

[42] Ndozangue-Touriguine, O., Sebbagh, M., Merino, D., Micheau, O. et al., A mitochondrial block and expression of XIAP lead to resistance to TRAIL-induced apoptosis during progression to metastasis of a colon carcinoma. *Oncogene* 2008, *27*, 6012–6022.

[43] Subauste, M. C., Ventura-Holman, T., Du, L., Subauste, J. S. et al., RACK1 downregulates levels of the pro-apoptotic protein Fem1b in apoptosis-resistant colon cancer cells. *Cancer Biol. Ther.* 2009, *8*, 2297–2305.

[44] Vishnubhotla, R., Sun, S., Huq, J., Bulic, M. et al., ROCK-II mediates colon cancer invasion via regulation of MMP-2 and MMP-13 at the site of invadopodia as revealed by multiphoton imaging. *Lab. Investigation; J. Techn. Methods Pathol.* 2007, *87*, 1149–1158.

[45] Zhang, B., Halder, S. K., Kashikar, N. D., Cho, Y. J. et al., Antimetastatic role of Smad4 signaling in colorectal cancer. *Gastroenterology* 2010, *138*, 969–980; e961–963.

[46] Shiou, S. R., Datta, P. K., Dhawan, P., Law, B. K. et al., Smad4-dependent regulation of urokinase plasminogen activator secretion and RNA stability associated with invasiveness by autocrine and paracrine transforming growth factor-beta. *J. Biol. Chem.* 2006, *281*, 33971–33981.

[47] Cantin, R., Diou, J., Belanger, D., Tremblay, A. M., Gilbert, C., Discrimination between exosomes and HIV-1: purification of both vesicles from cell-free supernatants. *J. Immunol. Methods* 2008, *338*, 21–30.

[48] Mathivanan, S., Lim, J. W., Tauro, B. J., Ji, H. et al., Proteomics analysis of A33 immunoaffinity-purified exosomes released from the human colon tumor cell line LIM1215 reveals a tissue-specific protein signature. *Mol. Cell. Proteomics* 2010, *9*, 197–208.

[49] Coleman, B. M., Hanssen, E., Lawson, V. A., Hill, A. F., Prion-infected cells regulate the release of exosomes with distinct ultrastructural features. *FASEB J.* 2012, *26*, 4160–4173.

[50] Barile, L., Gherghiceanu, M., Popescu, L. M., Moccetti, T., Vassalli, G., Ultrastructural evidence of exosome secretion by progenitor cells in adult mouse myocardium and adult human cardiospheres. *J. Biomed. Biotechnol.* 2012, 2012, 354605.

[51] Choi, D. S., Choi, D. Y., Hong, B. S., Jang, S. C. et al., Quantitative proteomics of extracellular vesicles derived from human primary and metastatic colorectal cancer cells. *J. Extracell. Vesicles* 2012, *1*, 18704.

[52] Baietti, M. F., Zhang, Z., Mortier, E., Melchior, A. et al., Syndecan-syntenin-ALIX regulates the biogenesis of exosomes. *Nat. Cell Biol.* 2012, *14*, 677–685.

[53] Hurley, J. H., Odorizzi, G., Get on the exosome bus with ALIX. *Nat. Cell Biol.* 2012, *14*, 654–655.

[54] Choi, D. S., Lee, J. M., Park, G. W., Lim, H. W. et al., Proteomic analysis of microvesicles derived from human colorectal cancer cells. *J. Proteome. Res.* 2007, *6*, 4646–4655.

[55] Pisitkun, T., Shen, R. F., Knepper, M. A., Identification and proteomic profiling of exosomes in human urine. *Proc. Natl. Acad. Sci. USA* 2004, *101*, 13368–13373.

[56] Sleeman, J. P., The metastatic niche and stromal progression. *Cancer Metastasis Rev.* 2012, *31*, 429–440.

[57] Castellana, D., Zobairi, F., Martinez, M. C., Panaro, M. A. et al., Membrane microvesicles as actors in the establishment of a favorable prostatic tumoral niche: a role for activated fibroblasts and CX3CL1-CX3CR1 axis. *Cancer Res.* 2009, *69*, 785–793.

[58] Nguyen, D. X., Bos, P. D., Massague, J. Metastasis: from dissemination to organ-specific colonization. *Nat. Rev. Cancer* 2009, *9*, 274–284.

[59] Minn, A. J., Gupta, G. P., Siegel, P. M., Bos, P. D. et al., Genes that mediate breast cancer metastasis to lung. *Nature* 2005, *436*, 518–524.

[60] Grange, C., Tapparo, M., Collino, F., Vitillo, L. et al., Microvesicles released from human renal cancer stem cells stimulate angiogenesis and formation of lung premetastatic niche. *Cancer Res.* 2011, *71*, 5346–5356.

[61] Gherardi, E., Birchmeier, W., Birchmeier, C., Vande Woude, G., Targeting MET in cancer: rationale and progress. *Nat. Rev. Cancer* 2012, *12*, 89–103.

[62] Birchmeier, C., Birchmeier, W., Gherardi, E., Vande Woude, G. F., Met, metastasis, motility and more. *Nat. Rev. Mol. Cell Biol.* 2003, *4*, 915–925.

[63] Grant, D. S., Kleinman, H. K., Goldberg, I. D., Bhargava, M. M. et al., Scatter factor induces blood vessel formation in vivo. *Proc. Nat. Acad. Sci. USA* 1993, *90*, 1937–1941.

[64] Abounader, R., Laterra, J., Scatter factor/hepatocyte growth factor in brain tumor growth and angiogenesis. *Neurooncology* 2005, *7*, 436–451.

[65] Jo, M., Stolz, D. B., Esplen, J. E., Dorko, K. et al., Cross-talk between epidermal growth factor receptor and c-Met signal pathways in transformed cells. *J. Biol. Chem.* 2000, *275*, 8806–8811.

[66] Kankuri, E., Cholujova, D., Comajova, M., Vaheri, A., Bizik, J., Induction of hepatocyte growth factor/scatter factor by fibroblast clustering directly promotes tumor cell invasiveness. *Cancer Res.* 2005, *65*, 9914–9922.

[67] Oskarsson, T., Acharyya, S., Zhang, X. H., Vanharanta, S. et al., Breast cancer cells produce tenascin C as a metastatic niche component to colonize the lungs. *Nat. Med.* 2011, *17*, 867–874.

[68] Matei, I., Ghajar, C. M., Lyden, D. A., TeNaCious foundation for the metastatic niche. *Cancer Cell* 2011, *20*, 139–141.

[69] Foo, S. S., Turner, C. J., Adams, S., Compagni, A. et al., Ephrin-B2 controls cell motility and adhesion during blood-vessel-wall assembly. *Cell* 2006, *124*, 161–173.

[70] Surawska, H., Ma, P. C., Salgia, R., The role of ephrins and Eph receptors in cancer. *Cytokine Growth Factor Rev.* 2004, *15*, 419–433.

[71] Liu, W., Ahmad, S. A., Jung, Y. D., Reinmuth, N. et al., Coexpression of ephrin-Bs and their receptors in colon carcinoma. *Cancer* 2002, *94*, 934–939.

[72] Liu, W., Jung, Y. D., Ahmad, S. A., McCarty, M. F. et al., Effects of overexpression of ephrin-B2 on tumour growth in human colorectal cancer. *Br. J. Cancer* 2004, *90*, 1620–1626.

[73] Yang, N. Y., Lopez-Bergami, P., Goydos, J. S., Yip, D., Walker, A. M. et al., The EphB4 receptor promotes the growth of melanoma cells expressing the ephrin-B2 ligand. *Pigment Cell Melanoma Res.* 2010, *23*, 684–687.

[74] Steinhoff, M., Brzoska, T., Luger, T. A., Keratinocytes in epidermal immune responses. *Curr. Opinion Allergy Clin. Immunol.* 2001, *1*, 469–476.

[75] Dhawan, P., Singh, A. B., Deane, N. G., No, Y. et al., Claudin-1 regulates cellular transformation and metastatic behavior in colon cancer. *J. Clin. Investigation* 2005, *115*, 1765–1776.

[76] Salama, I., Malone, P. S., Mihaimeed, F., Jones, J. L., A review of the S100 proteins in cancer. *Eur. J. Surgical Oncol.* 2008, *34*, 357–364.

[77] Stulik, J., Osterreicher, J., Koupilova, K., Knizek, Macela, A. et al., The analysis of S100A9 and S100A8 expression in matched sets of macroscopically normal colon mucosa and colorectal carcinoma: the S100A9 and S100A8 positive cells underlie and invade tumor mass. *Electrophoresis* 1999, *20*, 1047–1054.

[78] Rafii, S., Lyden, D., S100 chemokines mediate bookmarking of premetastatic niches. *Nat. Cell Biol.* 2006, *8*, 1321–1323.

[79] Yang, C., Robbins, P. D., The roles of tumor-derived exosomes in cancer pathogenesis. *Clin. Dev. Immunol.* 2011, 2011, 842–849.

[80] Polakis, P., Wnt signaling in cancer. *Cold Spring Harb. Perspect. Biol.* 2012, doi: 10.1101/cshperspect.a008052.

[81] Mahmoudi, T., Li, V. S., Ng, S. S., Taouatas, N. et al., The kinase TNIK is an essential activator of Wnt target genes. *EMBO J.* 2009, *28*, 3329–3340.

[82] Taira, K., Umikawa, M., Takei, K., Myagmar, B. E. et al., The Traf2- and Nck-interacting kinase as a putative effector of Rap2 to regulate actin cytoskeleton. *J. Biol. Chem.* 2004, *279*, 49488–49496.

[83] Kawabe, H., Neeb, A., Dimova, K., Young, S. M., Jr. et al., Regulation of Rap2A by the ubiquitin ligase Nedd4–1 controls neurite development. *Neuron* 2010, *65*, 358–372.

[84] Gloerich, M., ten Klooster, J. P., Vliem, M. J., Koorman, T. et al., Rap2A links intestinal cell polarity to brush border formation. *Nat. Cell. Biol.* 2012, *14*, 793–801.

[85] Nubel, T., Preobraschenski, J., Tuncay, H., Weiss, T. et al., Claudin-7 regulates EpCAM-mediated functions in tumor progression. *Mol. Cancer Res.* 2009, *7*, 285–299.

[86] Simons, K., van Meer, G., Lipid sorting in epithelial cells. *Biochemistry* 1988, *27*, 6197–6202.

[87] Patra, S. K., Dissecting lipid raft facilitated cell signaling pathways in cancer. *Biochimica et biophysica acta* 2008, *1785*, 182–206.

[88] Foster, L. J., De Hoog, C. L., Mann, M., Unbiased quantitative proteomics of lipid rafts reveals high specificity for signaling factors. *Proc. Natl. Acad. Sci. USA* 2003, *100*, 5813–5818.

[89] Staubach, S., Hanisch, F. G., Lipid rafts: signaling and sorting platforms of cells and their roles in cancer. *Expert Rev. Proteomics* 2011, *8*, 263–277.

[90] Lingwood, D., Simons, K., Lipid rafts as a membrane-organizing principle. *Science* 2010, *327*, 46–50.

[91] Simons, K., Gerl, M. J., Revitalizing membrane rafts: new tools and insights. *Nat. Rev. Mol. Cell Biol.* 2010, *11*, 688–699.

[92] Stuermer, C. A., The reggie/flotillin connection to growth. *Trends Cell. Biol.* 2010, *20*, 6–13.

[93] Patel, H. H., Murray, F., Insel, P. A., G-protein-coupled receptor-signaling components in membrane raft and caveolae microdomains. *Handbook Exp. Pharmacol.* 2008, *186*, 167–184.

[94] Bertolini, G., Roz, L., Perego, P., Tortoreto, M. et al., Highly tumorigenic lung cancer CD133+ cells display stem-like features and are spared by cisplatin treatment. *Proc. Natl. Acad. Sci. USA* 2009, *106*, 16281–16286.

[95] Rasheed, Z. A., Matsui, W., Biological and clinical relevance of stem cells in pancreatic adenocarcinoma. *J. Gastroenterol. Hepatol.* 2012, 27 (Suppl 2), 15–18.

[96] Vander Griend, D. J., Karthaus, W. L., Dalrymple, S., Meeker, A. et al., The role of CD133 in normal human prostate stem cells and malignant cancer-initiating cells. *Cancer Res.* 2008, *68*, 9703–9711.

[97] Zhang, Z., Filho, M. S., Nor, J. E., The biology of head and neck cancer stem cells. *Oral Oncol.* 2012, *48*, 1–9.

[98] Huttner, H. B., Corbeil, D., Thirmeyer, C., Coras, R. et al., Increased membrane shedding–indicated by an elevation of CD133-enriched membrane particles–into the CSF in partial epilepsy. *Epilepsy Res.* 2012, *99*, 101–106.

[99] Fargeas, C. A., Karbanova, J., Jaszai, J., Corbeil, D., CD133 and membrane microdomains: old facets for future hypotheses. *World J. Gastroenterol.* 2011, *17*, 4149–4152.

[100] Lathia, J. D., Hitomi, M., Gallagher, J., Gadani, S. P. et al., Distribution of CD133 reveals glioma stem cells self-renew through symmetric and asymmetric cell divisions. *Cell Death Dis.* 2011, *2*, e200.

[101] Rappa, G., Fodstad, O., Lorico, A., The stem cell-associated antigen CD133 (Prominin-1) is a molecular therapeutic target for metastatic melanoma. *Stem Cells* 2008, *26*, 3008–3017.

[102] Patra, S. K., Dissecting lipid raft facilitated cell signaling pathways in cancer. *Biochim. Biophys. Acta.* 2008, *1785*, 182–206.

[103] Koga, K., Matsumoto, K., Akiyoshi, T., Kubo, M. et al., Purification, characterization and biological significance of tumor-derived exosomes. *Anticancer Res.* 2005, *25*, 3703–3707.

[104] Qu, J. L., Qu, X. J., Zhao, M. F., Teng, Y. E. et al., Gastric cancer exosomes promote tumour cell proliferation through PI3K/Akt and MAPK/ERK activation. *Digestive Liver Dis.* 2009, *41*, 875–880.

